JOURNAL OF COMPUTATIONAL PHYSICS **138,** 695–713 (1997)
ARTICLE NO. CP975839

Evaluation of Two Lattice Boltzmann Models for Multiphase Flows

Shuling Hou,* Xiaowen Shan,* Qisu Zou,*,‡ Gary D. Doolen,* and Wendy E. Soll†

**Theoretical Division and †Earth and Environmental Sciences Division, Los Alamos National Laboratory, Los Alamos, New Mexico 87545; and ‡Department of Mathematics, Kansas State University, Manhattan, Kansas 66506*

Received July 22, 1996

Two lattice Boltzmann models for multiphase flows, the immiscible fluid model proposed by Rothman and Keller (R–K) and the multicomponent nonideal gas lattice Boltzmann model by Shan and Chen (S–C), are studied numerically to compare their abilities to simulate the physics of multiphase flows. The test problem is the simulation of a static bubble. Isotropy, strength of surface tension, thickness of the interface, spurious currents, Laplace's law, and steadiness of the bubble are examined. The results show that the S–C model is a major improvement over the R–K model.

1. INTRODUCTION

The lattice Boltzmann Equation (LBE) method has recently emerged as a powerful tool of computational fluid dynamics, especially for the simulation of complex fluids. Based on the lattice gas automata (LGA), the LBE method inherited most of the advantages of the LGA and eliminated the excessive statistical noise and the lattice artifacts such as the lack of Galilean invariance and the dependence of the pressure on the fluid velocity. In the LBE method, particle distribution functions for particles with a set of fixed velocities are evolved by a lattice Boltzmann equation on a regular lattice. The (macroscopic) fluid density and velocities averaged from the particle distribution satisfy the Navier–Stokes equations, which can be derived by applying a Chapman–Enskog procedure to the lattice Boltzmann equation. Readers are referred to [1–3] and the references therein for details of these methods.

The LBE method is of spherical significance for the numerical simulation of complex fluids, e.g., muiltiphase flows. Microscopically, the segregation of a fluid

0021-9991/97 $25.00

system into different phases is due to the interparticle forces. While these particle–particle interactions are difficult to implement in traditional methods, they can be naturally taken into account in numerical methods based on the simulation of the motion of particles or particle distributions. The crucial step in developing a LBE multiphase model is to incorporate correctly the particle interaction into the evolution of the particle distribution functions so that macroscopically correct multiphase flow behavior can be simulated.

The first lattice gas model for immiscible two-phase flow was proposed by Rothman and Keller in 1988 [4]. Based on the single-phase triangular FHP model, two kinds of colored particles, red and blue, are introduced for two phases. A local flux and color field (color gradient) are calculated and the work of the color flux against the field minimum is chosen to encourage the preferential grouping of like colors. Although this model is the pioneering work for two-phase flow using lattice gas automata, it is not practical, at least not quantitatively, because it inherits the noisy nature and other defects of the lattice gas method. The two-phase lattice Boltzmann model proposed by Gunstensen *et al.* [5, 6] is based on the original Rothman–Keller lattice gas model combining the lattice Boltzmann method of McNamara and Zanetti [7] with the linearized collision operator proposed by Higuera and Jimenez [8]. Although the unphysical properties like the lack of Galilean invariance and statistical noise are overcome, the pressure is still velocity dependent. In addition, the linearized collision operator is not computationally efficient and the model cannot handle two fluids with different densities and viscosities [9]. Grunau *et al.* [9, 10] further developed the model with the collision operator simplified by using the single-time relaxation approximation with a proper particle equilibrium distribution function. The comparison conducted below is based on the work of Grunau *et al.* The two-phase lattice Boltzmann models mentioned above are all based on the Rothman–Keller lattice gas model. We therefore refer to it as the R–K model.

The lattice Boltzmann model proposed by Shan and Chen [11–14] introduces a non-local interaction between particles at neighboring lattice sites. An arbitrary number of components, up to the limit imposed by the available amount of computer memory, with different molecular masses can be simulated in this model. Interaction potentials are defined for each of the components, which control the form of the equation of state of the fluid. The fluid or fluid mixture separates into different phases depending upon the interaction potentials. Their model is labeled here as the S–C model. The two models will be described briefly in order to understand their different mechanisms for simulating two-phase flows.

The basic requirement for a LBE model to be practically useful is that it has to be able to produce a steady-state interface with a surface tension satisfying Laplace's law. From the point of view of practical usage, the isotropy of the surface tension and the thickness of the interface are important properties. It is also preferable to have a surface tension which can be made as strong as possible. Based on these criteria, the problem of simulating a static bubble was selected as our test problem.

The two lattice Boltzmann models used here are otherwise identical except for the particle–particle interaction. They are both three dimensional and with 14 velocity directions $\mathbf{e}_i$, $i = 1, ..., 14$. A cubic lattice with unit spacing (lattice unit) is used in which each node has 6 nearest neighbors and 8 next-nearest neighbors

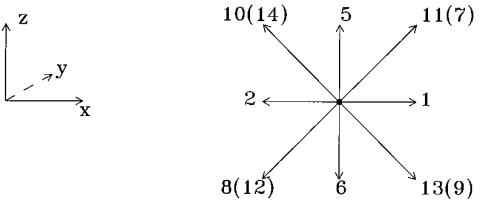

FIG. 1. Schematic plot of velocity directions of the 3-D lattice model. The y-axis is pointing into the paper, so are velocity directions 3, 7, 9, 12, 14 (they are in parentheses if shown), while the velocity directions 4, 8, 10, 11, 13 are pointing out. Velocity directions 3, 4 have a projection at the center and are not shown in the figure.

connected by a total of 14 links. Particles can only reside on the nodes and move to their nearest and next-nearest neighbors along these links during each unit time step. There are rest particles (type 0) with zero velocity ($\mathbf{e}_0 = 0$) and two types of moving particles. Particles of type 1 (the ones with velocity $\mathbf{e}_i$, $i = 1, ..., 6$, e.g., $\mathbf{e}_1 = (1, 0, 0)$) move along the directions of xyz-coordinate axes with speed 1 and particles of type 2 (the ones with velocity $\mathbf{e}_i$, $i = 7, ..., 14$, e.g., $\mathbf{e}_7 = (1, 1, 1)$) move along the diagonal directions with speed $\sqrt{3}$. A 2-D projection of the velocities to the xz plane is shown in Fig. 1. The population of particles with velocity $\mathbf{e}_i$ is represented by the single particle distribution function $f_i(\mathbf{x}, t)$.

The rest of this paper is organized as follows. First, the R–K and the S–C models will briefly be described in Sections 2 and 3, respectively. The testing problem, the range of parameters, the setup of the testing conditions, and the results are presented in Section 4. Finally, a discussion and conclusions are given in Section 5.

2. R–K MODEL

In this section, a brief description of the R–K model is given. The two fluids denoted by different colors, say, red and blue, obey the lattice Boltzmann equation

$$f_i^k(\mathbf{x} + \mathbf{e}_i, t + 1) - f_i^k(\mathbf{x}, t) = \Omega_i^k(\mathbf{x}, t), \qquad \text{where } i = 0, ..., 14, \tag{1}$$

where $f_i^k(\mathbf{x}, t)$ is the particle distribution in the ith velocity direction for the kth fluid (red or blue) at position $\mathbf{x}$ and time t. These particle distributions are evolved by Eq. (1). The (macroscopic) density of kth fluid is calculated from $f_i^k(\mathbf{x}, t)$ as $\rho_k(\mathbf{x}, t) \equiv \sum_{i=0}^{14} f_i^k(\mathbf{x}, t)$. The total density is $\rho(\mathbf{x}, t) = \sum_k \rho_k(\mathbf{x}, t)$. The (macroscopic) local velocity $\mathbf{v}$ is defined as $\rho(\mathbf{x}, t)\mathbf{v}(\mathbf{x}, t) \equiv \sum_k \sum_{i=1}^{14} \mathbf{e}_i f_i^k(\mathbf{x}, t)$. The collision operator, Ω_i^k, can be split into two parts. The first part denoted by $(\Omega_i^k)^1$ is the same as the BGK single-phase collision term [15] and can be simplified as [15–18]

$$(\Omega_i^k)^1 = -\frac{1}{\tau_k}[f_i^k(\mathbf{x}, t) - f_i^{k(eq)}(\mathbf{x}, t)], \tag{2}$$

where $f_i^{k(eq)}(\mathbf{x}, t)$ is the equilibrium distribution at $\mathbf{x}$, t and τ_k is the single-relaxation time for the kth fluid. The second part of the collision operator for the 3-D 15-direction model is given as

$$(\Omega_i^k)^2 = A|\mathbf{F}|\left[\frac{(\mathbf{e}_i \cdot \mathbf{F})^2}{|\mathbf{e}_i|^2 * |\mathbf{F}|^2} - \frac{1}{3}\right], \tag{3}$$

where A is an adjustable parameter. Its range and effect on the surface tension will be discussed in the next section. $\mathbf{F}$ is the local gradient defined as

$$\mathbf{F}(\mathbf{x}, t) = \sum_i \mathbf{e}_i[\rho_r(\mathbf{x} + \mathbf{e}_i, t) - \rho_b(\mathbf{x} + \mathbf{e}_i, t)]. \tag{4}$$

The R–K model also applies a so-called ''recolor'' procedure near the interface at the collision step [5, 6, 10]. Because of this ''recolor'' procedure, particles of one color tend to congregate together. Thus, R–K model forces the two fluids to be immiscible. The equilibrium distribution of the species k as functions of $\mathbf{x}$, t is given for both the R–K and the S–C model as

$$\begin{aligned}
f_0^{k(eq)} &= \rho_k\left(\frac{\lambda_k}{7 + \lambda_k} - \frac{1}{3}v^2\right), \text{(type 0)} \\
f_i^{k(eq)} &= \rho_k\left[\frac{1}{7 + \lambda_k} + \frac{1}{3}(\mathbf{e}_i \cdot \mathbf{v}) + \frac{1}{2}(\mathbf{e}_i \cdot \mathbf{v})^2 - \frac{1}{6}v^2\right], \qquad i = 1, ..., 6 \text{ (type 1)} \\
f_i^{k(eq)} &= \frac{\rho_k}{8}\left[\frac{1}{7 + \lambda_k} + \frac{1}{3}(\mathbf{e}_i \cdot \mathbf{v}) + \frac{1}{2}(\mathbf{e}_i \cdot \mathbf{v})^2 - \frac{1}{6}v^2\right], \qquad i = 7, ..., 14 \text{ (type 2)},
\end{aligned} \tag{5}$$

where λ_k is a parameter representing the ratio of rest and type 1 particles of the kth fluid when velocity $\mathbf{v}$ is zero. v is the magnitude of $\mathbf{v}$. $f_i^{k(eq)}$ satisfy $\rho_k = \sum_{i=0}^{14} f_i^{k(eq)}$ and $\rho_k\mathbf{v} = \sum_{i=1}^{14} \mathbf{e}_i f_i^{k(eq)}$. It is assumed in the R–K model that $\rho_r/(7 + \lambda_r) = \rho_b/(7 + \lambda_b) \equiv d$ [9]. Hence, the density ratio of two fluids can be expressed as

$$\gamma = \frac{\rho_r}{\rho_b} = \frac{7 + \lambda_r}{7 + \lambda_b}.$$

In a pure kth phase, ρ_k and $\mathbf{v}$ satisfy the Navier–Stokes equations. The viscosity is given by $\nu_k = (2\tau_k - 1)/6$. The R–K model has an ideal-gas equation of state based on the fact that pressure is proportional to the density for red and blue particles, i.e., $p_k = c_k^2\rho_k$ where c_k, ρ_k, and p_k are the speed of sound, density, and pressure of the kth (red or blue) component, respectively (based on the single-phase result). The sound speeds of the model used in the test are $c_r^2 = 3/(7 + \lambda_r)$ for the red fluid and $c_b^2 = 3/(7 + \lambda_b)$ for the blue fluid. The Reynolds number of a LBE simulation is given by $\mathrm{Re} = UN/\nu_k$, where U is a characteristic velocity and N is the number of lattice unit in a characteristic length L. This relation establishes a connection of the lattice unit and the physical unit. If two flows have the same

Re number, then their nondimension form of the equations are the same, so does the nondimensional time. Thus, if $T_1(T_2)$, $L_1(L_2)$, and $U_1(U_2)$ are the characteristic time, length, and velocity of the flow system 1 (2) where systems 1, 2 correspond to a physical system and the LBE, respectively, we have $t_1/(L_1/U_1) = t_2/(L_2/U_2)$, so $t_1 = (L_1U_2/L_2U_1)t_2$. For example, if $U_2 = 0.12$ (in lattice unit), $U_1 = 0.12$ cm/s, $L_2 = 10$ (e.g., the radius of a bubble is 10 lattice units), $L_1 = 5$ cm (the radius of a bubble is 5 cm in the physical problem), then $t_1 = 0.5t_2$ s.

In addition to the parameter A in Eq. (3), Grunau *et al.* [10] introduced several other free parameters. The second part of the collision operator $(\Omega_i^k)^2$ given by Eq. (3), the so-called binary-fluid perturbation, is in effect only when the magnitude of the color gradient is greater than a threshold, ε. To continuously connect relaxation parameters τ_r and τ_b at an interface, a parameter δ is introduced to make a smooth transition of two viscosities within a distance δ from the interface.

3. S–C MODEL

The multicomponent multiphase LBE model proposed by Shan and Chen [11–14] also uses the BGK collision term. The particle distribution functions $f_i^k(\mathbf{x}, t)$ (the population of particles) of an arbitrary number of components with molecular mass m_k are allowed. The interaction between the particles of different components are included in the kinetics through a set of potentials. With the same notation, the lattice Boltzmann equations for the kth component can be written in the same form as Eq. (1), with the collision term being

$$\Omega_i^k(\mathbf{x}, t) = -\frac{1}{\tau_k}[f_i^k(\mathbf{x}, t) - f_i^{k(eq)}(\mathbf{x}, t)]. \tag{6}$$

The index k runs from 1 to S, the total number of components, which is only limited by the available computer memory. The density of the kth fluid is defined as $\rho_k(\mathbf{x}, t) \equiv m_k \sum_i f_i^k(\mathbf{x}, t)$, the fluid velocity of the kth fluid $\mathbf{v}_k$ is defined through $\rho_k\mathbf{v}_k \equiv m_k \sum_i \mathbf{e}_i f_i^k$ (m_k are equal to one in our study). The equilibrium distribution functions are the same as given in Eq. (5) except the velocity $\mathbf{v}$ is replaced by the equilibrium velocity $\mathbf{v}_k^{(eq)}$ given by the relation

$$\rho_k\mathbf{v}_k^{\mathrm{eq}} = \rho_k\mathbf{v}' + \tau_k\mathbf{F}_k, \tag{7}$$

where $\mathbf{v}'$ is a common velocity on top of which, an extra component-specific velocity due to interparticle interaction is added for each component. $\mathbf{F}_k$ is the total interparticle force acting on the kth component to be given below. Thus, in this model, interaction of particles is through the equilibrium distribution. To conserve momentum at each collision in the absence of interaction (i.e., in the case of $\mathbf{F}_k = 0$), $\mathbf{v}'$ has to satisfy the relation

$$\mathbf{v}' = \left(\sum_{k=1}^{S} \frac{\rho_k\mathbf{v}_k}{\tau_k}\right) \Bigg/ \left(\sum_{k=1}^{S} \frac{\rho_k}{\tau_k}\right). \tag{8}$$

Hence, given f_i^k, ρ_k, and $\mathbf{v}_k$ can be calculated, and then so can $\mathbf{v}'$, $\mathbf{v}_k^{(eq)}$, and $f_i^{k(eq)}$. The interaction force between particles of the kth component at site $\mathbf{x}$ and the k'th component at site $\mathbf{x}'$ is assumed to be proportional to the product of their "effective mass" $\psi_k(\rho_k)$ defined as a function of local density. The total interaction force on the kth component at site $\mathbf{x}$ is

$$\mathbf{F}_k(\mathbf{x}) = -\psi_k(\mathbf{x}) \sum_{\mathbf{x}'} \sum_{\bar{k}=1}^{S} G_{k\bar{k}}(\mathbf{x}, \mathbf{x}')\psi_{\bar{k}}(\mathbf{x}')(\mathbf{x}' - \mathbf{x}), \tag{9}$$

where $G_{k\bar{k}}(\mathbf{x}, \mathbf{x}')$ is a Green's function and satisfies $G_{k\bar{k}}(\mathbf{x}, \mathbf{x}') = G_{k\bar{k}}(\mathbf{x}', \mathbf{x})$. $\psi_k(\mathbf{x})$ is a function of $\mathbf{x}$ through its dependence of ρ_k. If only homogeneous isotropic interactions between the nearest neighbors are considered, $G_{k\bar{k}}(\mathbf{x}, \mathbf{x}')$ can be reduced to the following symmetric matrix with constant elements,

$$G_{k\bar{k}}(\mathbf{x}, \mathbf{x}') = \begin{cases} 0, & |\mathbf{x} - \mathbf{x}'| > c, \\ g_{k\bar{k}}, & |\mathbf{x} - \mathbf{x}'| \le c. \end{cases} \tag{10}$$

Here $g_{k\bar{k}}$ is the strength of the interaction potential between component k and $\bar{k}$. c is the lattice spacing (1 in lattice unit). The effective mass $\psi_k(\rho_k)$ is taken as ρ_k in this study; other choices will give a different equation of state. The total mass density of the whole fluid is defined as $\rho = \sum_k \rho_k$, and the whole fluid velocity $\mathbf{v}$ is defined by $\rho\mathbf{v} = \sum_k \rho_k\mathbf{v}_k + \frac{1}{2}\sum_k \mathbf{F}_k$.

The Chapman–Enskog method has been applied to the above lattice Boltzmann equation to derive a set of macroscopic equations for each component, which is very similar to the Navier–Stokes equations [13, 14]. The pressure in the 3-D 15-direction model is given by $p = \frac{1}{3}\rho + \frac{3}{2}\sum_{k,\bar{k}} g_{k,\bar{k}}\psi_k\psi_{\bar{k}}$, which represents a nonideal gas law. The viscosity is given by $\nu = \frac{1}{3}(\sum_k \alpha_k\tau_k - \frac{1}{2})$, where α_k is the mass concentration of the kth component defined as ρ_k/ρ [13, 14]. ν is reduced to $(2\tau_k - 1)/6$ in a region of pure kth component.

With the inclusion of interparticle interactions, the collision operator does not conserve total particle momentum at each site. However, the total momentum of the whole system is still conserved. Effectively the interaction introduces an extra momentum transfer flux among the lattice sites. This is probably the most important microscopic difference between the S–C and the R–K models.

4. BUBBLE TEST

The test physical problem selected in a 2-D (in the xy-plane) static circular bubble of radius r_0 of one fluid immersed in another fluid. The center of the circle is at the center of the computational xy-plane. In the equilibrium state with no body force, each fluid has a constant density and pressure with zero velocities. Across the interface, there is a pressure jump determined by the radius of the bubble and the surface tension given by Laplace's law $\Delta p = \sigma/r_0$ (because it is actually a cylindrical bubble in the 3-D space). We want to look at the bubble shape, the surface tension, and Laplace's law from the simulations at steady state. Since LBE

is a dynamical procedure, the state of a static bubble is achieved through a time evolution and the size of the final bubble and final densities are unknown at the initial time. The dynamical evolution of a bubble from a nonequilibrium state to an equilibrium state is not the intended physical phenomenon to simulate. Because the two LBE models used are 3-D lattice model, the variables are set uniform in the z-direction to simulate a cylindrical bubble with the circular section in the xy-plane. The lattice size is $65 \times 65 \times 3$ with the center of the bubble located at (33, 33, 2). Periodic boundary conditions are applied in all three coordinate directions.

4.1. *Setup of the Test*

To implement the LBE models, first particle distributions f_i^k have to be initialized. Then the density ρ_k and velocities $\mathbf{v}$ (in the R–K model) or $\mathbf{v}_k^{(eq)}$ (in the S–C model) are obtained, so are $f_i^{k(eq)}$. Equation (1) is used to evolve f_i^k. At each step, the density ρ_k (hence the pressure) and velocities $\mathbf{v}$ are obtained as the flow variables to approximate the physical problem. In the bubble simulations, if the relative difference of the maximum magnitude of the velocities at a time step T and at $T - 100$ is smaller than a tolerance (say, 10^{-5}), steady state is considered to be achieved (in this case, all other variables have a small relative change less than the tolerance). If steady state cannot be reached, the simulation time is 40,000 steps in lattice units. We then compare the results in the final stage. Since the two models have different mechanisms and parameters for simulating two-phase flows, the ways of initialization are not the same. In addition, it is difficult to force the same bubble radius and densities in the final stage for two models because these quantities are not known before the simulation. However, we have tried to choose the same parameters for the two models if possible and we have trid to initialize suitably so that initial bubble radii are the same and in the final stage the average densities of the bubble fluid of the two models are close for a reasonable comparison. The bubble is formed mainly by red particles (R–K model) or phase 0 (S–C model). Outside the bubble, blue particles (R–K) or phase 1 (S–C) are dominant. Parameters involved in both models are λ_r, λ_b, τ_r, and τ_b (we assume that r, b are replaced by 0, 1, respectively, for the S–C model; their meaning is discussed in Section 2). We choose $\lambda_r = \lambda_b = 2$, $\tau_r = \tau_b = 1$ and $\lambda_0 = \lambda_1 = 2$, $\tau_0 = \tau_1 = 1$ (for the S–C model). From these, the sound of speed c_s is given by $c_s^2 = 1/3$ for both models according to the discussion in Section 2. For the R–K model, other parameters are given by $A = 0.01$, $\varepsilon = 0.75$ (since $\lambda_r = \lambda_b$, the parameter δ used to smoothly connect λ_r and λ_b does not play any role). The reason for choosing these parameters will be discussed in next subsection. For the S–C model, the remaining parameter is the strength of the interaction potential, $g_{k\bar{k}}$. We use $g_{01} = g_{10} = g = 0.2$.

For the R–K model, initial particle distributions inside and outside a cylinder with radius $r_{init} = 10$ centered in the computational domain are purely red and purely blue, respectively. In each region of pure phase k, the initial distributions f_i^k for $i = 1, ..., 6$ are given by a constant $d = d_0 = 0.28$ plus a small random perturbation; f_0^k is given by $\lambda_k d_0$ plus a small random perturbation; and f_i^k for $i = 7, ..., 14$ are given by $d_0/8$ plus a small random perturbation as in [5, 6, 10]. The density ρ_k and velocity $\mathbf{v}$ can be obtained, so are $f_i^{k(eq)}$. In this way, the initial

TABLE I
Effect of Parameter A in the R–K Model ($\varepsilon = 0.75$, $d_0 = 0.3$, $r_{init} = 10$)

A	σ	$\lvert\mathbf{v}\rvert_{max}$	Width
0.01	0.330	0.118	3
0.001	0.0322	0.012	2
0.0001	0.0032	0.0012	2

densities (and the pressure) inside and outside the bubble are close to 2.52 with some small random perturbation. Note that there should be no blue particle distribution over the region of the bubble; otherwise some small blue bubbles will be formed inside the large red bubble, rendering a different physical situation. For the S–C model, on the other hand, there must be a small amount of phase 1 fluid inside the initial bubble and a small amount of phase 0 fluid outside, as otherwise the simulation blows up. So the initialization must be different from that of the R–K model. For the S–C model, initially, inside and outside the initial bubble with $r_{init} = 10$, density of phase 0, ρ_0, is set uniformly to 2.093 and 0.0638, respectively, and ρ_1 is set uniformly to 0.0524 and 2.011, respectively. Velocity $\mathbf{v}_k^{(eq)}$ is set to zero, and f_i^k are set to $f_i^{k(eq)}$ calculated from ρ_k and $\mathbf{v}_k^{(eq)}$. From this initialization, the initial pressure of both models does not balance the surface tension. Hence, the initial bubble evolves. In the final stage, the resulted bubbles from the two models have radii around 10 and the average densities of the bubble fluid of the two models are very close to make a reasonable comparison.

4.2. *Parameter Range*

The parameter choice in the previous subsection is based on some tests of the interfacial properties such as surface tension, maximum color gradient, maximum magnitude of velocity, spatial extent of the spurious currents, and pressure profile in the xy-plane.

For the R–K model, as the value of ε varies from 0.2 to 5.0, respectively, the values of surface tension, maximum velocity, and maximum color gradients do not change. When $\varepsilon = 5.0$, however, the maximum color gradients in x- and y-directions at the same time step are slightly different, indicating a clear anisotropy. While the maximum color gradients in the x- and y-directions are about 13, they vary from 0.9 to 1.6 in the z-direction for different values of ε (for $A = 0.01$).

The parameter A in Eq. (3) is an important one for the R–K model. The surface tension is almost proportional to A. Simulations with $A = 0.02$, 0.01, 0.001, and 0.0001 were tested with other free parameters unchanged. Relative to $A = 0.01$, $A = 0.001$ and 0.0001 give thinner interfaces and smaller velocities of spurious currents and smaller surface tensions. For $A = 0.02$, the bubble changes its shape periodically in time. The magnitude of the velocity is about 0.26, which is too large for the lattice Boltzmann simulation. The values of surface tension, maximum velocity, and width of the interface for the different values of A are listed in Table I.

In the S–C model, that the two fluids are immiscible is only an extreme case. When g is smaller than 0.2, the two fluids are miscible, as indicated by the density plots which show that phase 0 fluid inside the bubble has a uniform nonzero density outside the bubble. The density ratio between densities inside and outside the bubble can be over 500 for $g = 0.2$, indicating that the two fluids are almost immiscible. Thus, in this study, the S–C model should have the value of g to be at least 0.2. Simulations for larger values of g (such as $g = 0.22$ or more) cause the simulation to blow up.

4.3. *Test Results*

Simulations for both models were performed on the Los Alamos CM-5. The results are analyzed as follows.

The simulation starts with an initial bubble with radius 10, without balance of pressure difference and the surface tension, the bubble evolves and should reach a steady state. However, for the R–K model, the radius of the bubble changes to around 9.81 in less than 100 steps and then oscillates all the time and no real steady state is reached with the tolerance of 10^{-5}. The simulation is stopped at 40,000 time steps. In this final stage, a bubble of radius about 9.81 is formed with the variation of the radius with time being less than 0.01 (approximately static with about 0.1% relative variation). The maximum magnitude of the velocities oscillates with time in the interval [0.1174, 0.1202] (about 2.4% relative variation). In the final stage, the averaged red particle density (over the whole region) is 0.1891. For the S–C model, the radius oscillates somewhat in the first 200 time steps and then is monotonically increasing to the final steady value of 10.48 at about 20,000 steps. The simulation is continued to time steps of 40,000 for comparison. The steady-state-averaged density of phase 0 over the whole computational region is 0.1853. Thus, both models yield a final static bubble (only approximately static for the R–K model), giving an approximation to the physical problem. The details of the results and the deviations of the simulations from the physical problem will be discussed in the following items.

A. Spurious currents and oscillations of variables in the final stage. Figures 2 and 3 are velocity vector plots in the xy-plane at $z = 2$ (the symmetry plane) in the final stage for the R–K and the S–C model, respectively. Although there may be some small relative fluctuations as time evolves, they represent the typical behavior of the velocity field. The magnitude of the velocity $\mathbf{v}$ is represented by the length of the arrows, which have the same scale for both figures. The nonzero velocity field in these figures represents the deviation of the results of both models from the physical problem. The steady-state velocity field is most pronounced in the interface region. These nonzero velocities are called spurious currents. For the cases compared, the spurious currents are much more serious in the R–K model than in the S–C model. While the spurious currents are mostly constrained to be in the interface region in the S–C model, they extend to a distance far away from the interface in the R–K model. The lattice effect is very obvious in the R–K model because the spurious currents have much more strength along the lattice directions (i.e., in the directions of $(\pm 1, 0)$, $(0, \pm 1)$, $(\pm 1, \pm 1)$). The maximum velocity is about

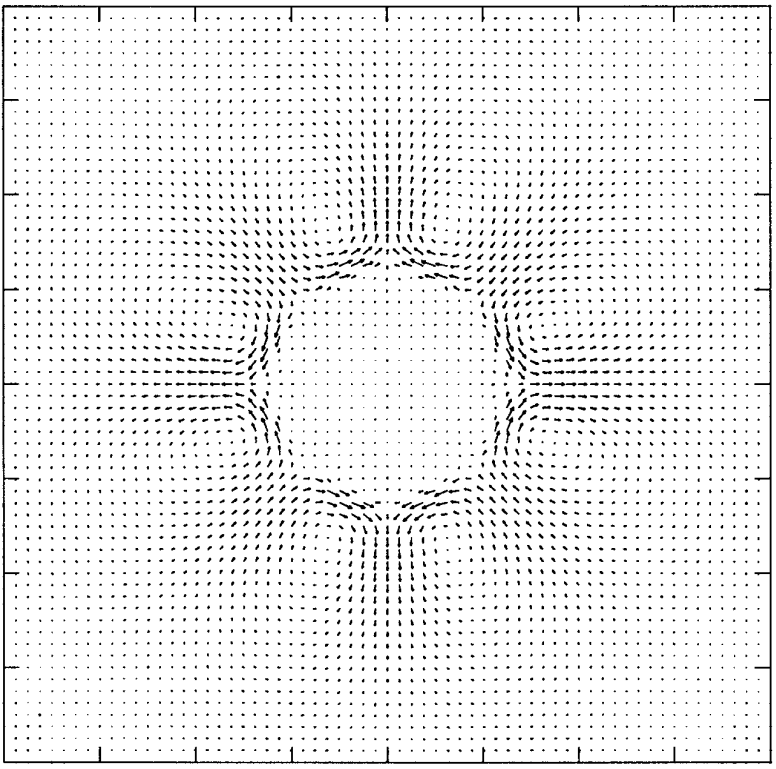

FIG. 2. Velocity vector plot in the xy-plane at $z = 2$ (the symmetry plane) for the R–K model.

0.12 in the R–K model and 0.059 in the S–C model for the case tested. Considering that the velocity in the lattice Boltzmann method should be small (usually 0.1 or smaller for incompressible flow), the value of 0.12 is about the same magnitude of a typical velocity field and is too large for obtaining meaningful results. The spurious currents are closely related to the value of A in the R–K model and can be reduced using smaller values of A, but the surface tension decreases accordingly. In the S–C model, the spurious currents can also be reduced by reducing the values of g, generating higher miscibility.

Spurious currents at the interface are also present for some more conventional methods, for example, in the continuum surface force model [19].

In the final stage, the variables in the R–K model still oscillate while the variables in the S–C model are very steady. To see this, a time series of quantities like the maximum magnitude of the velocity, the maximum and minimum of density of two components, the surface tension, the radius of the bubble, and the center of the bubble are studied. As an example, Figures 4 and 5 are plots for relative variations of the maximum magnitude of velocity versus time. The maximum magnitude of velocity among all nodes, $|\mathbf{v}|_{max}$, at every 100 time steps is taken, the mean of which is calculated as $\bar{v}$, which is about 0.12 and 0.059 for the R–K and the S–C models, respectively, then the quantity $(|\mathbf{v}|_{max} - \bar{v})/\bar{v}$ is plotted in Figures 4 and 5 for the R–K and the S–C models, respectively. This value oscillates randomly all the time

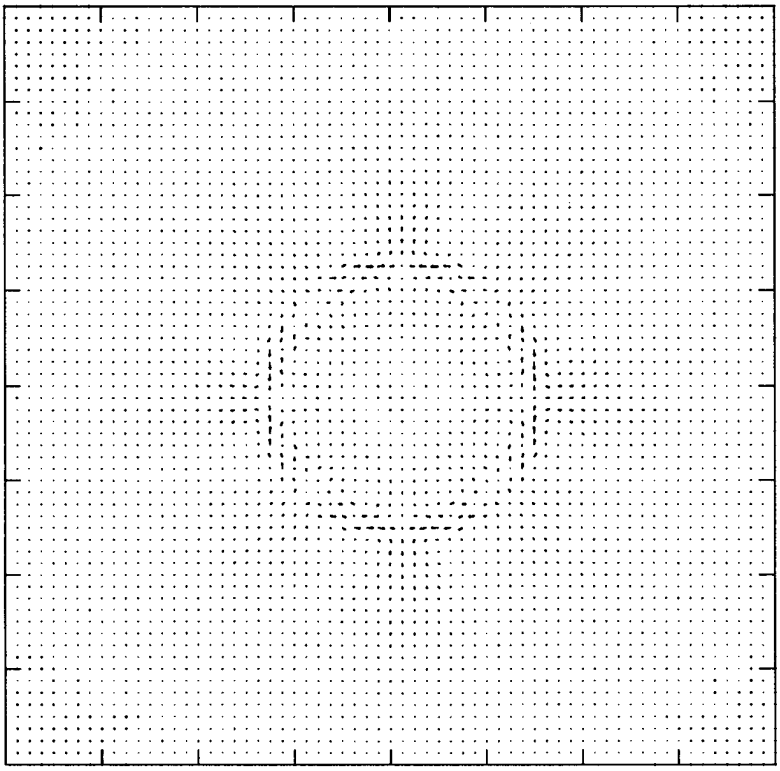

FIG. 3. Velocity vector plot in the xy-plane at $z = 2$ (the symmetry plane) for the S–C model.

for the R–K model while the S–C model has a decay mechanism and reaches a steady state. Note that the velocity in the final stage is not physical itself; the purpose of Figs. 4 and 5 is only to indicate the ability of the methods to reach the steady state.

B. Isotropy. Figures 2 and 3 also show that the velocities in the R–K and the S–C models are symmetric with respect to all *lattice* directions. However, they are not symmetric with respect to all directions as in the physical problem. The R–K model is obviously more anisotropic. For example, in Fig. 2, along the ray from the center of the bubble in the x-direction and along the ray which forms an angle of 22.5° with the x-direction, the velocities have different behavior especially near the interface. To examine isotropy more clearly, ρ_r and ρ_b at each node are plotted versus the radius measured from the center of the bubble; this is shown in Figs. 6 and 7 for the R–K model and the S–C model (where ρ_0, ρ_1 are plotted), respectively. For each computational node with indices (i, j, k), its radius R is given by $R = \sqrt{(i-33)^2 + (j-33)^2}$, and two values ρ_r and ρ_b are plotted (these two dots should be far apart in the same vertical direction). Since the lattice is square in the xy-plane, four different nodes will have the same value of R. If the model is isotropic, all four ρ_r values corresponding to the same R should have the same dot in the plot (ρ_b should have another dot), and the values of ρ_r for nodes with very close R values should be very close. Figure 7 for the S–C model shows this isotropy property almost everywhere, except the outer area of the bubble where slightly

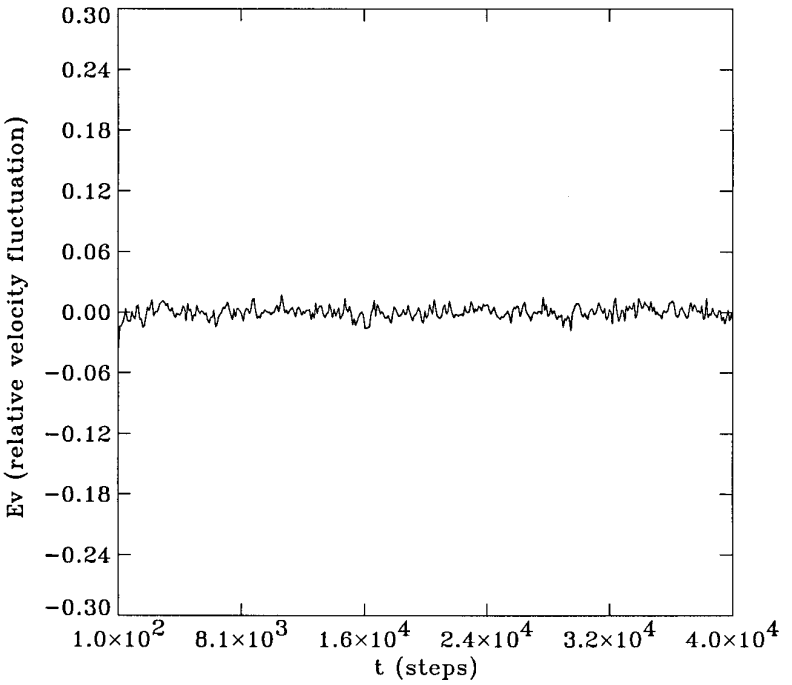

FIG. 4. Time history of relative maximum velocity fluctuation, $(|\mathbf{v}|_{max} - \bar{v})/\bar{v}$, where $\bar{v}$ is the time averaged of $|\mathbf{v}|_{max}$, for the R–K model.

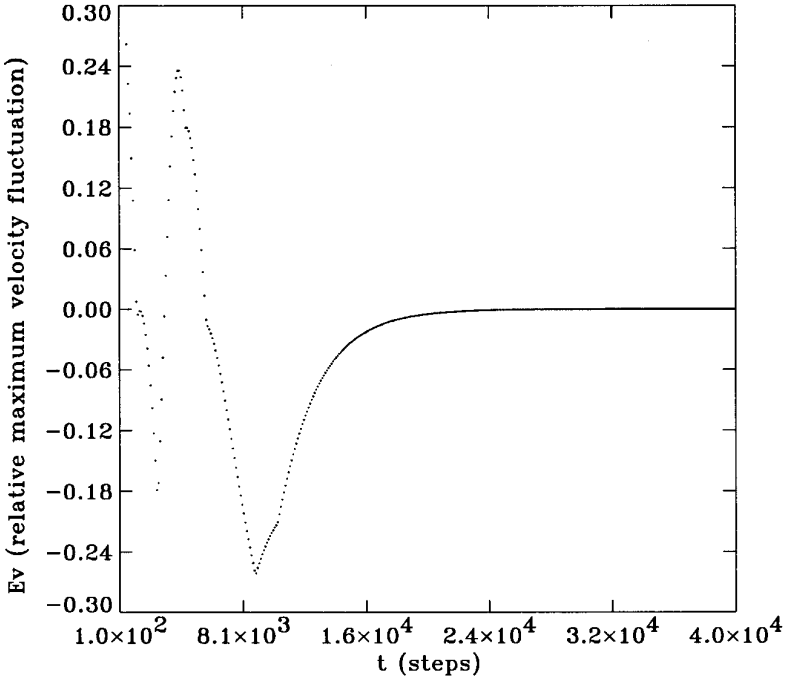

FIG. 5. Time history of relative maximum velocity fluctuation $(|\mathbf{v}|_{max} - \bar{v})/\bar{v}$, where $\bar{v}$ is the time averaged of $|\mathbf{v}|_{max}$, for the S–C model.

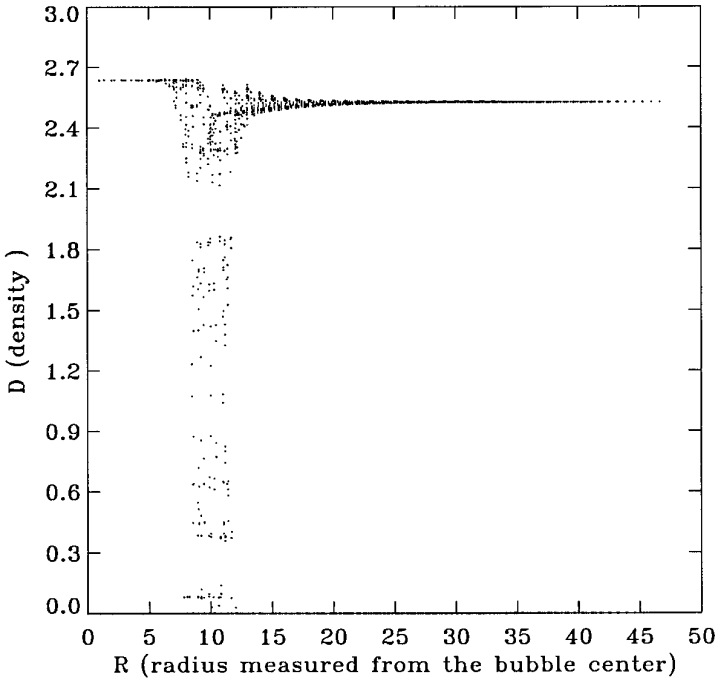

FIG. 6. Density versus the radius measured from the center of the bubble for the R–K model.

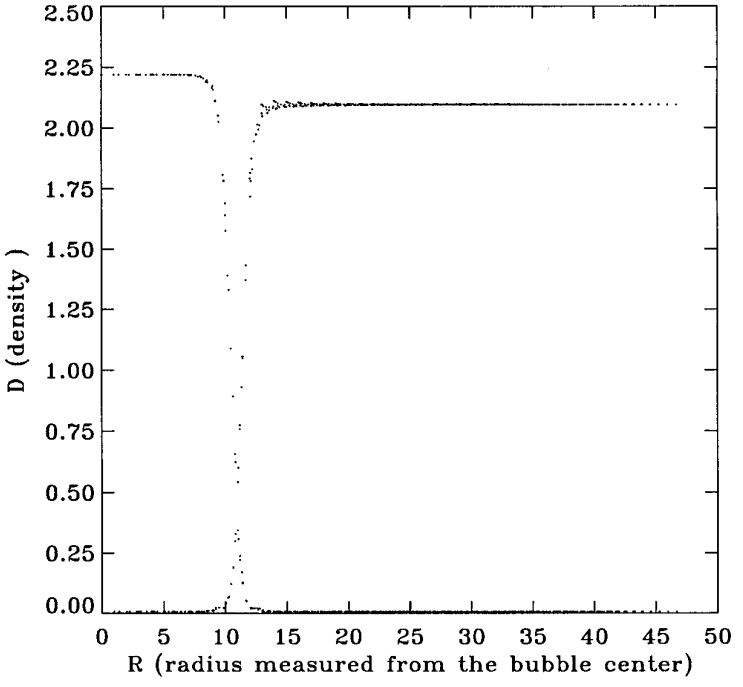

FIG. 7. Density versus the radius measured from the center of the bubble for the S–C model.

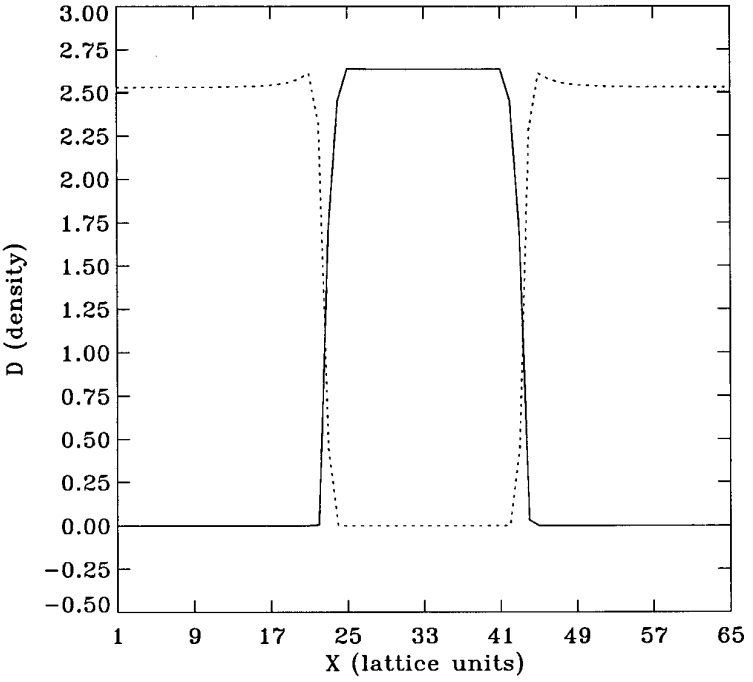

FIG. 8. The density profiles in the symmetry plane ($z = 2$) along the central line ($y = 33$) for the R–K model. (——) Red. (· · ·) Blue.

spread spots appear. In contrast with Fig. 7, Fig. 6 shows a poor isotropy of the R–K model. An anisotropy is clearly seen in the interface region. Figures 8 and 9 and the discussion in the following subsection give a better idea about the density profiles along a ray.

C. Thickness of the interface. Physically the thickness of the interface between two fluids is on the order of angstroms. However, this is not obtainable with existing numerical methods. The thickness of the interface can be measured using the density (or pressure) variation across the interface. The density profiles in the symmetry plane ($z = 2$ in this test) along the central line ($y = 33$) are plotted versus the x-axis for both models, as shown in Figs. 8 and 9. Figure 8 shows that the density of the red (blue) has a maximum (minimum) value inside (outside) the bubble. The zero density of red (blue) well outside (well inside) the bubble indicates that the R–K model is an immiscible model. The width of the sharp gradient between the maximum and minimum values of the red density is defined as the thickness of the interface. For the R–K model, this is about 3 lattice units for the test case. The thickness of the interface can be reduced further using a smaller value of A, but the surface tension decreases proportionally. Figure 9 shows the density profile for the S–C model at the same position as Fig. 8 and gives about the same thickness of the interface as the R–K model. It is seen from these two figures that, while the density of component 1 outside the interface in the S–C model is a constant, the density of blue particles in the R–K model is a constant far from the interface and

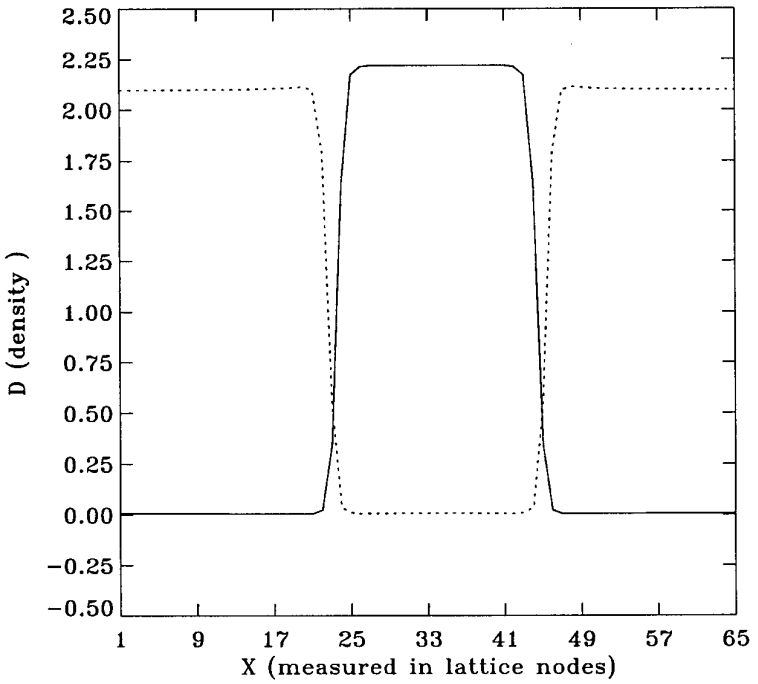

FIG. 9. The density profiles in the symmetry plane ($z = 2$) along the central line ($y = 33$) for the S–C model. (——) Component 0. (· · ·) Component 1.

has a tendency to match the red density inside the bubble near the interface before drops down to zero. The pressure profiles for both models give similar results.

Since the interface has a finite thickness, to study Laplace's law, we define the radius of the bubble in the final stage, R, through the formula

$$\rho_{max}\pi R^2 + (L^2 - \pi R^2)\rho_{min} = \bar{\rho}L^2, \tag{11}$$

where $L^2 = nx \times ny$ is the total area of the computational xy-region, $\bar{\rho} \equiv \sum \rho_r/(nx \times ny \times nz)$ is the average density of the bubble fluid (red or phase 0), the sum is over all i, j, k. ρ_{max} and ρ_{min} are the maximum and minimum of ρ_r over the whole computational domain. It is obvious that ρ_{max} is reached inside the bubble and ρ_{min} is reached outside the bubble. This definition states that the bubble radius is such that if the bubble fluid density is uniformly ρ_{max} inside the bubble and uniformly ρ_{min} outside the bubble, then the total density of bubble fluid from this configuration is equal to the actual total bubble fluid density.

D. Surface tension. In the final stage of the simulations, pressure and the bubble radius R can be determined. The surface tension, σ, is calculated according to Laplace's law,

$$p_i - p_o = \frac{\sigma}{R}, \tag{12}$$

TABLE II
Test of Laplace's Law for the R–K Model ($A = 0.001$, $d_0 = 0.29$)

Radius:	7.89	10.02	11.82	14.99	19.95
σ:	0.0363	0.0361	0.0343	0.0315	0.0198
Δp:	0.0046	0.0036	0.0029	0.0021	0.0099

where p_i and p_o are pressures inside and outside the bubble. The values of the pressure inside (outside) should be a constant theoretically. Since the thickness of the interface is finite and both phases exist near the interface, the values of pressure vary near the interface. For this reason, p_i and p_o are taken away from the interface.

The surface tension obtained is about 0.346 for the R–K model for a radius of 9.81. The surface tension is 0.446 for the S–C model with radius 10.48. Based on these figures and Laplace's law, the surface tension for radius equal to 10 is 0.352 for the R–K model and 0.424 for the S–C model. The surface tension calculated here is in lattice units and can be related to practical problems. The surface tensions calculated are *a posteriori* in the R–K model. For the S–C model the numerical value of the surface tension for the *single-component liquid–vapor* model was obtained analytically in [12]. This depends on the functional form of the potential and the strength of the interaction. In the modeling of multiphase problems, the dimensionless numbers of the LBE fluid, such as the capillary number, the weber number, etc., therefore can be determined from the surface tension.

E. Laplace's law. To test Laplace's law given in Eq. (12) for both models, simulations with different initial bubbles are performed, and the final radius R and the pressure differences are recorded. These results are listed in Tables II and III and plotted in Figs. 10 and 11 for the R–K and the S–C model, respectively. It is found that the parameter $A = 0.01$ in the R–K model causes the bubble with radius 20 to be unstable and to change shape periodically. The value of A therefore used in the test of Laplace's law is 0.001 and the initial density for moving particles along the axes is $d_0 = 0.29$. The + signs indicate results of the lattice Boltzmann simulations and the solid line is the least-square linear fit through the origin. These figures clearly show differences between the models. In Fig. 11, all points representing radius from 8 to 20 fit a straight line. The pressure difference inside and outside the bubble is indeed proportional to the reciprocal of the radius for the S–C model. Unfortunately, this is not the case for the R–K model. At larger radii, the deviation from a straight line is very obvious. This may be caused by the fact that the spurious currents extend far away from the interface in the R–K model. Since periodic boundary conditions are applied for the test bubble, an array of bubbles is being simulated. For large radii and fixed lattice size, the nonzero velocity fields between bubbles may interact and cause Laplace's linear relation to fail.

F. Computing time and memory. The computations were performed on the CM5. If 32 processors are used for $65 \times 65 \times 3$ lattice, the CPU time for updating 100 time steps including only streaming and relaxation is 8.9 s for the R–K model and 10.1 s for the S–C model. The memory required is 61.9 megabytes for the R–K model and 62.4 megabytes for the S–C model.

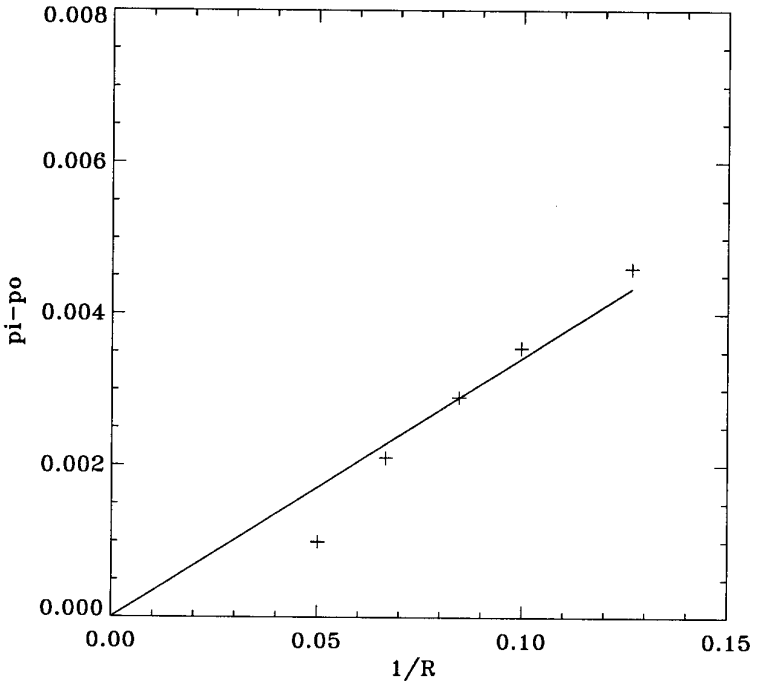

FIG. 10. Test of Laplace's law for the R–K model ($A = 0.001$, $d_0 = 0.29$).

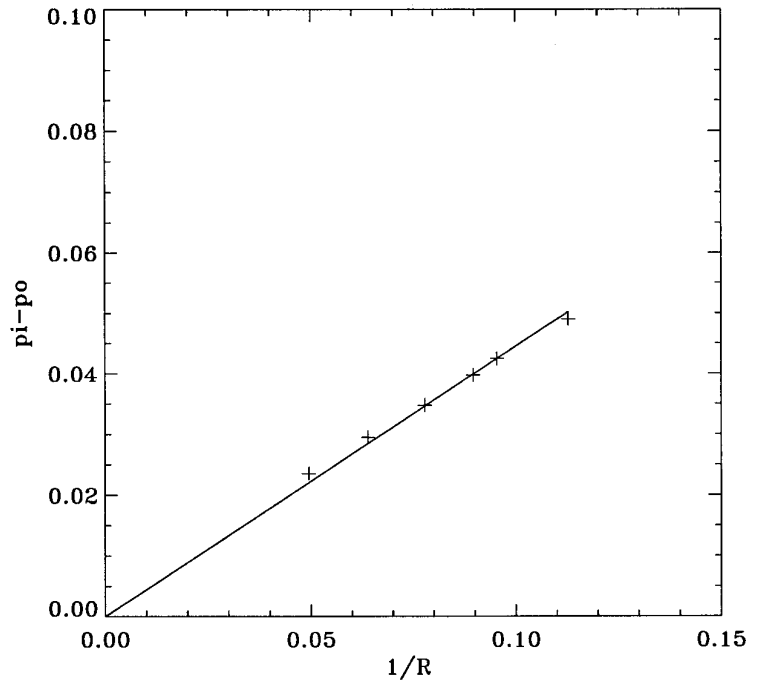

FIG. 11. Test of Laplace's law for the S–C model.

TABLE III
Test of Laplace's Law for the S–C Model

Radius:	8.87	10.48	11.16	12.85	15.64	20.20
σ:	0.4346	0.4454	0.4442	0.4472	0.4614	0.4747
Δp:	0.0490	0.0425	0.0398	0.0348	0.0295	0.0235

5. CONCLUSIONS

Two lattice Boltzmann models for two-phase flows, the R–K model and the S–C model, are evaluated and analyzed for their ability to simulate a static bubble. Two models are both based on the same lattice Boltzmann equation and single-relaxation-time assumptions. Hence, they share some advantages, such as being efficient for massively parallel computing and easy handling of complicated boundaries. The results demonstrate that although both models can simulate, to a certain degree, complex interfacial phenomena, the abilities of the two models to simulate two-phase flows are much different. While a physically correct isotropic, stable bubble satisfying Laplace's law can be simulated by the S–C model, it is poorly represented by the R–K model. The S–C model can simulate larger surface tensions and maintain smaller spurious currents in both magnitude and range than the R–K model. The thickness of the interface and computing time and memory are about the same for two models.

It is of interest to give a preliminary analysis of the reasons why the R–K model performs unsatisfactorily. Since the spurious currents and the oscillations occur even for a plane interface for the R–K model, they cannot be attributed to the loss of isotropy in the discretization of the space. It is believed that the reason lies in the way the particle–particle interaction is microscopically modeled. In the R–K model, interactions between particles exist in an arbitrarily defined ''interfacial zone'' and the strength is calculated through a maximization process which in our tests seems to have failed to give converging results. The small parameter, ε, that defines the interfacial zone does not have correspondence with physical quantities. While the formation of the surface tension through binary-fluid perturbation and the segregation of the two phases through the maximization process are achieved in two separate steps for the R–K model, these two physical phenomena are completed spontaneously as consequences of the same physical mechanism in the S–C model. Moreover, since the interaction is added unphysically only in the interfacial zone, the bulk of the two phases still satisfies the equation of state of an ideal gas which in reality does not have phase transitions of any kind.

Despite a necessary step, the simple static bubble test conducted here is certainly not sufficient to establish the LBE with the S–C model as a mature computational method for simulating multiphase flows. More detailed benchmark results in other flow configurations, especially with dynamic flows, are called for and more simulation results will be reported in future publications.

ACKNOWLEDGMENTS

Discussions with Daryl W. Grunau, John Rodgers, and Xiaoyi He are appreciated. Special thanks to J. U. Brackbill for helpful suggestions. The code used in the paper for the R-K model was written by Daryl Grunau. The authors acknowledge the Advanced Computing Laboratory of Los Alamos National Laboratory for providing use of the CM-5. Q. Z. thanks David Sharp for providing a summer support and acknowledges NSF Grant DMR-9413513 and NSF-EPSCoR Grant OSR 9550487.

REFERENCES

1. U. Frisch, B. Hasslacher, and Y. Pomeau, *Phys. Rev. Lett.* **56,** 1505 (1986).
2. G. D. Doolen (Ed.), *Lattice Gas Methods for Partial Differential Equations,* (Addison–Wesley, 1989).
3. S. Hou, Q. Zou, S. Chen, G. D. Doolen, and A. C. Cogley, *J. Comput. Phys.* **118,** 329 (1995).
4. D. H. Rothman and J. M. Keller, *J. Stat. Phys.* **52,** 1119 (1988).
5. A. K. Gunstensen, D. H. Rothman, S. Zaleski, and G. Zanetti, *Phys. Rev. A* **43,** 4320 (1991).
6. A. K. Gunstensen and D. H. Rothman, *Europhys. Lett.* **18,** 157 (1992).
7. G. G. McNamara and G. Zanetti, *Phys. Rev. Lett.* **61,** 2332 (1988).
8. F. Higuera and J. Jimènez, *Europhys. Lett.* **9,** 663 (1989).
9. D. Grunau, Ph.D. Thesis, Colorado State University, 1993.
10. D. Grunau, S. Chen, and K. Eggert, *Phys. Fluids A* **5,** 2557 (1993).
11. X. Shan and H. Chen, *Phys. Rev. E* **47,** 1815 (1993).
12. X. Shan and H. Chen, *Phys. Rev. E* **49,** 2941 (1994).
13. X. Shan and G. D. Doolen, *J. Stat. Phys.* **49,** 2941 (1995).
14. X. Shan and G. D. Doolen, *Phys. Rev. E* **54,** 3614 (1996).
15. P. L. Bhatnagar, E. P. Gross, and M. Krook, *Phys. Rev.* **94,** 511 (1954).
16. S. Chen, H. Chen, D. Martinez, and W. H. Matthaeus, *Phys. Rev. Lett.* **67,** 3776 (1991).
17. Y. Qian, D. d'Humières, and P. Lallemand, *Europhys. Lett.* **17,** 479 (1992).
18. H. Chen, S. Chen, and W. H. Matthaeus, *Phys. Rev. A* **45,** 5339 (1992).
19. J. U. Brackbill, D. B. Kothe, and C. Zemach, *J. Comput. Phys.* **100,** 335 (1992).